Novel Hierarchical Control of VSI-based Microgrids Against Large-Signal Disturbances

M. Fazli[1] **M. A. Hejazi[2]**
[1] Master Degree Graduate, Department of Electrical and Computer Engineering,
University of Kashan, Kashan, Iran
m.fazli@grad.kashanu.ac.ir
[2] Assistant Professor, Department of Electrical and Computer Engineering,
University of Kashan, Kashan, Iran
mhejazi@kashanu.ac.ir

Abstract :

This paper provides a novel hierarchical control for VSI-based microgrids. The advantage of the provided control scheme is to maintain the frequency and voltage stability and load sharing against large-signal disturbances. A hierarchical control, consisting of three levels, is described. A new control loop based on PI controller, is presented. The new control loop has a great impact on increasing the stability margins, by moving the poles. In next steps, secondary and tertiary control levels are described. Then, the voltage droop equation is improved by a fuzzy controller. This controller generates a floating reactive power reference value, by a fuzzy logic. The role of floating reactive power reference value is to compensate the drastic changes in the voltage amplitude by changing the reactive power reference value. To verify the performance of the provided control scheme, a microgrid including four VSI-based DGs is simulated in islanded and grid-connected modes, by MATLAB/ SIMULINK. The simulation results show that the micogrid can maintain the frequency and voltage stability, in term of large-signal disturbances such as 3-phase and 1-phase short circuits. With this method microgrid load sharing is not altered after disturbances.

Keywords: Droop Control, Fuzzy Control, Hierarchical Control, Large-signal Disturbance, Microgrid, Power Sharing, Stability, Voltage Source Inverter (VSI).

Submission date: 22, 08, 2016

Acceptance date: 23, 11, 2016

Corresponding author: M. A. Hejazi

Corresponding author's address: University of Kashan, Ghotb Ravandi Blvd. 6km, Kashan, Iran.

1. Introduction

The restrictions of the transmission lines in remote areas and economic and environmental problems of bulk power generation, predispose to reach the restructured electricity system. Distributed generation (DG) and smart grids play an important role for the establishment of a restructured electricity grid and microgrids.

The future distribution networks can be imagined as a number of interconnected microgids in which every user can be responsible for the generation, storage and consumption of energy, and can share the energy with neighbors, in the form of a smart grid [1]-[2].

Several control strategies have been developed for microgrid controls, including natural droop control, modified natural droop control, hierarchical control, and virtual droop control. Modified natural droop control has gained widespread recognition, and a resilient version of this concept is discussed in [3].

Power electronics plays an important role to achieve this revolutionary technology. In fact, the power electronic devices are used as interface of DGs, energy storage systems and loads with microgrids and in this way; Voltage-Source Inverters (VSI) are frequently utilized.

The control of parallel VSIs connected to a microgrid is an important issue that several studies have been conducted on it in recent years. The control of microgrids is based on droop control. The droop control method is derived from conventional power systems with synchronous generators in which any change in the active and reactive power cause changes in frequency and voltage variations, respectively. In energy resources such as fuel cells, solar cells and microturbines that are connected to the system through converters, the frequency of the output is naturally independent of the output power [4]-[5].

In this situation, VSIs can be controlled using two approaches, centralized or decentralized control. The centralized control is based on communication links similar to the Master-Slave method. In [6], a Master-Slave strategy is proposed for controlling the microgrid voltage. In decentralized control, each unit is controlled by its local controller which is not aware of the whole system disturbances. This approach is based on frequency and amplitude droop control [7]-[9]. The advantages of avoiding telecommunications-based control make the droop control as a competitive method to control microgird, although it does not guarantee a constant voltage amplitude and frequency. Hierarchical control scheme is a compromise between centralized and decentralized controls. In power systems, hierarchical control is consisting of three levels of control: primary, secondary and tertiary [1], [10].

In the field of the decentralized control of microgrids, many papers have been conducted for active and reactive power sharing, by controlling two quantities, frequency and voltage of the system [1]-[5] and [9]. In [4], [9] and [11] the inner control loops have been designed based on PI controllers, so that, in [12] the PR controllers is used. Some of them such as [13]-[15], attempt to improve stability by eigenvalues analysis. The communication link effect between DGs is analyzed in [16]-[19]. In [20]-[23] micogrid controller has been strong against the changes of loads and references values, by robust controllers. The relationship between power angle and active power has been utilized for the power sharing in [24]-[25]. The angle control has the advantage that during islanding operation, power sharing can be performed without changing the system frequency.

One of the drawbacks in droop-based control methods is that in the islanded mode, the voltage and frequency of the microgrid change with changes in load. Therefore, after the changes in load, a mechanism should be existing to restore the system frequency and voltage to nominal values [11] and [26]-[27]. This restoration mechanism is known as secondary control of voltage and frequency, and occurs over a longer time scale. In order to improve the reliability and performance of VSIs controlled by droop controller, virtual impedance control loops have been presented in [28]-[30].

The accuracy of load sharing and reactive power sharing is improved in [31] for droop controlled microgrid by error reduction operation and recovery of voltage. Also, damping factor is used for power flow analysis in [32]. Finally, all of the advantages and drawbacks of the droop control methods considering different droop parameters is discussed in [33].

A major issue discussed in all earlier research is the microgrid normal operation mode and small-signal studies, while no solution has been represented regarding the controller which should work well after occurrence of a large-signal disturbance, and also maintains the stability of the system to guarantee the desired power sharing.

In a microgrid, located in a rural or in a remote area the large-signal disturbances, such as short circuit, lightning, outage of lines between DG units and heavy motor starting can cause blackout and negative consequences. Therefore, providing the control that ensures microgrid operation is of particular importance. In this paper, a novel hierarchical control scheme is provided, in which a new controller in the inner control loops is added, and also reactive power reference will be controlled by a fuzzy logic controller. The presented

control scheme is tested by applying large-signal disturbances.

2. Inner -Control Loops / Primary Control

Fig. 1 indicates a sample microgird including two DGs. The DG units have DC voltage energy resource and supply a nonlinear load through VSI. This microgrid can be utilized in both islanded and grid-connected modes.

2.1. Droop Control

The proposed control for parallel VSIs in primary control level in microgrid is based on droop control, which is responsible for adjusting the frequency and the amplitude of the voltage reference v_{ref} according to distribution of real and reactive powers (P, Q). The well-known characteristics of the droop control are defined, as follows [7]-[9]:

$$\begin{aligned} \omega &= \omega^* - G_P(s)\cdot\left(P - P^*\right) \\ E &= E^* - G_Q(s)\cdot\left(Q - Q^*\right) \end{aligned} \tag{1}$$

where ω and E are, respectively, the frequency and the amplitude of the output voltage, so that ω^* and E^* are known as their reference values. Active and reactive powers are given by P and Q, and P^* and Q^* designate their reference values. $G_P(s)$ and $G_Q(s)$ are the transfer functions of the droop control as follows:

$$G_P(s) = s.\left(k_{pP} + \frac{k_{iP}}{s}\right), \qquad G_Q(s) = k_{pQ} \tag{2}$$

where k_{iP} and k_{pQ} are static droop parameters, and k_{pP} can be considered as system virtual inertia and also known as a transient droop term. k_{iP} is equal to the maximum frequency deviation divided by the nominal active power and k_{pQ} is equal to the maximum voltage amplitude deviation divided by the nominal reactive power [12].

As it is shown in Fig. 1, by using Clarke transformation [34] and transforming three phase values into $\alpha\beta$ coordinates, the instantaneous power values are calculated as follows:

$$\begin{aligned} p &= v_{c\alpha}\cdot i_{o\alpha} + v_{c\beta}\cdot i_{o\beta} \\ q &= v_{c\beta}\cdot i_{o\alpha} - v_{c\alpha}\cdot i_{o\beta} \end{aligned} \tag{3}$$

In the above equations, $v_{c\alpha\beta}$ and $i_{o\alpha\beta}$ are, respectively, the capacitor voltage and output current in $\alpha\beta$ coordinates. Then passing through a low pass filter with cutoff frequency ω_c, the values of the active and reactive powers can be obtained [4]- [5]:

$$P = \frac{\omega_c}{s+\omega_c}\cdot p, \qquad Q = \frac{\omega_c}{s+\omega_c}\cdot q \tag{4}$$

In addition, the primary control level can include virtual impedance loops which normally ensure the inductive behavior at the line-frequency (Fig. 1). Despite the fact that the series impedance of a synchronous generator is mainly inductive, the virtual impedance can be selected arbitrarily [1]-[2]. Here the values of the inductor and resistor in the virtual impedance are L_{vi} and R_{vi}, respectively, and we have [12]:

$$\begin{aligned} v_{vi\alpha} &= R_{vi}\cdot i_{o\alpha} + \omega L_{vi}\cdot i_{o\beta} \\ v_{vi\beta} &= R_{vi}\cdot i_{o\beta} + \omega L_{vi}\cdot i_{o\alpha} \end{aligned} \tag{5}$$

2.2. Inner Control Loops

Comprehensive models for internal control loops have been presented in [4]-[5], [11] and [12]. The presented model in [4]-[5], [11] includes the voltage and current control loops containing all feed-back and feed-forward terms. Output voltage and current are obtained with a standard proportional/integral controller.

In [12], the current and voltage control loops are provided on the basis of the proportional/resonant (PR) controller. In addition to these two control loops, the virtual impedance loop is provided at primary control level. Considering the better performance of this model compared to other ones, the internal control loops presented in this paper is based on this model.

As seen in Fig. 1, after LC filter, there is one output inductor. Inner control loops considered for each VSI are based on $\alpha\beta$ reference frame, voltage control loop, current control loop and an additional new control loop. The given voltage and current control loops include PR terms adjusted for the fundamental frequency, 5th, 7th and 11th harmonics. Due to the need to suppress voltage harmonics caused by nonlinear loads, not only current control loops but also voltage control loop is involved in pursuing current harmonics in order to feed nonlinear loads. The transfer functions of the voltage controller, $G_v(s)$ and the current controller, $G_i(s)$ are modeled as follows:

$$G_v(s) = k_{pV} + \sum_{h=1,5,7,11} \frac{k_{rhV}\,s}{s^2 + (\omega_o h)^2} \tag{6}$$

$$G_i(s) = k_{pI} + \sum_{h=1,5,7,11} \frac{k_{rhI}\,s}{s^2 + (\omega_o h)^2} \tag{7}$$

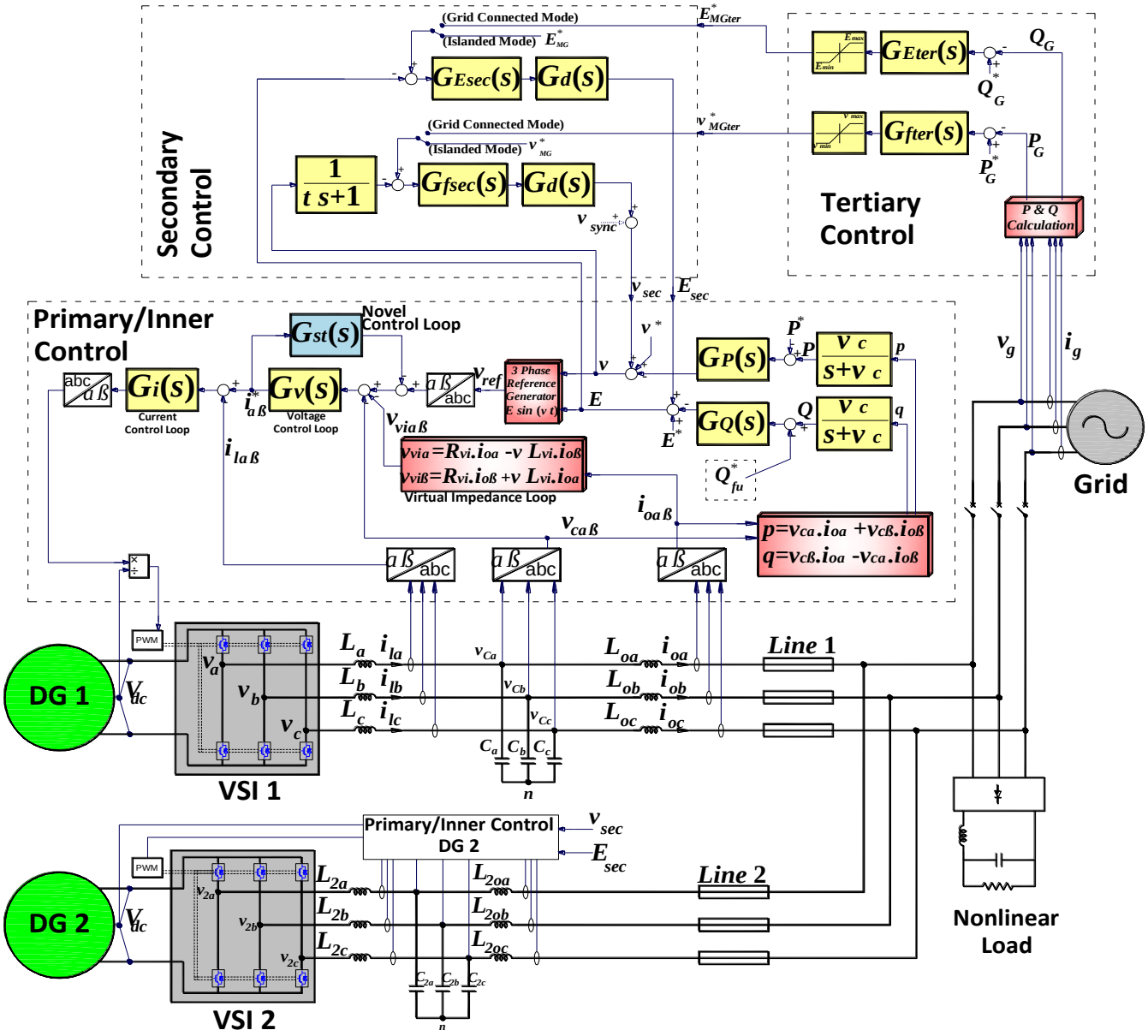

Fig. 1. Hierarchical control block diagram of micro-grid including two DGs and nonlinear load.

where $\omega_o=2\pi f$ and, k_{pV} and k_{pI} are, respectively, the proportional term parameters of voltage and current controllers. The voltage and current controller resonant term factors are k_{rhV} and k_{rhI}, respectively, which in the fundamental frequency, h is equal to 1 and for other harmonics h is equal to 5, 7 and 11 [12].

The new control loop proposed in this paper, gets the feedback from the voltage control loop. The controller consisting a PI term, is indicated in the microgrid control block diagram (Fig. 1) with the transfer function $G_{st}(s)$ and is defined as follows:

$$G_{st}(s)=k_{pst}+\frac{k_{ist}}{s} \qquad (8)$$

where k_{pst} and k_{ist} are, respectively, the proportional and integral term parameters of the new control loop transfer function. The controller significantly reduces the resonance effects caused by the voltage controller resonant terms so that, in addition to preserving the effectiveness of these resonant terms in following harmonics, the stability margin is also increased by this controller to a sufficient degree. Fig. 2 shows the bode diagram of the voltage control loop transfer function $G_v(s)$ of [12] without new control loop, and voltage control loop transfer function with the new control loop transfer function $G_v(s)/(1+G_v(s).G_{st}(s))$. Also, the root locus plot and situation of poles of these two transfer functions can be compared in Fig. 3a/b. It can be seen by applying the new control loop, the distance between the poles and the imaginary axis is increased. The performed simulations demonstrate that by adding this controller, not only in confronting with small-signal

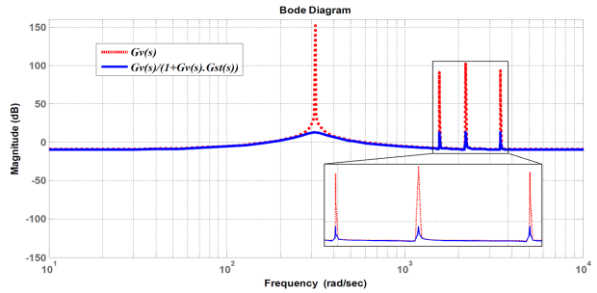

Fig. 2. Bode diagram of $G_v(s)$ and $G_v(s)/(1+G_v(s).G_{st}(s))$ (for listed parameters of table 1)

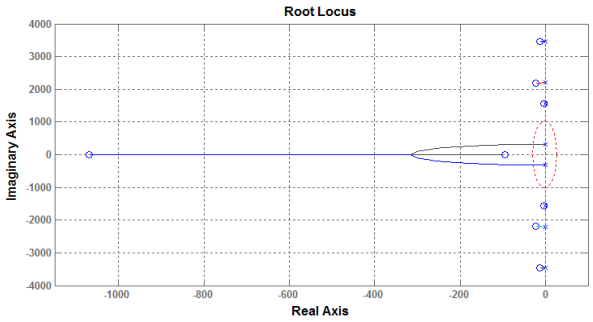

Fig. 3(a). Root locus plot of $G_v(s)$ (for listed parameters of table 1)

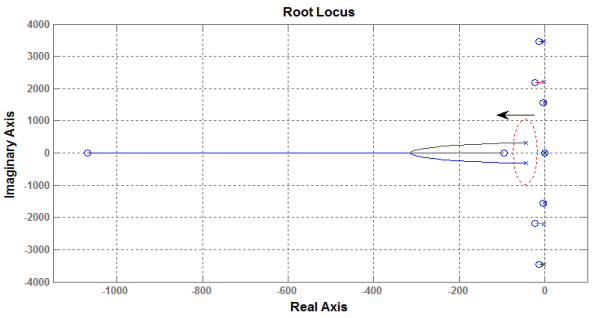

Fig. 3(b). Root locus plot of $G_v(s)/(1+G_v(s).G_{st}(s))$ (for listed parameters of table 1)

events but also against large-signal disturbances, the microgrid maintains its stability.

Fig. 4 shows the poles tracing of $G_v(s)/(1+G_v(s).G_{st}(s))$ for changes in k_{pst} from 0 to 10. Similarly, the poles tracing of the mentioned transfer function is shown in Fig. 5, for k_{ist} changes from 0 to 1000. There are two important points in design of the new control loop. First, the parameters should be chosen to increase the distance between poles and the imaginary axis for increasing stability. Second, the resonant terms should not be destroyed. In other words, a compromise should be performed between "reducing effectiveness of resonant terms in tracking harmonics", and "increasing stability".

3. Secondary Control

In order to compensate the frequency and voltage amplitude deviations, a secondary controller for the microgrid must be used. The secondary control ensures that the frequency and voltage deviations are reached towards zero after changes in load or generation. A PI controller is utilized. The equations of the secondary control can be achieved as follows:

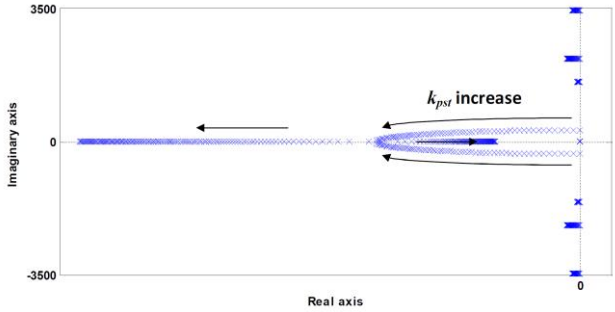

Fig. 4. Poles tracing of $G_v(s)/(1+G_v(s).G_{st}(s))$ for k_{pst} from 0 to 10.

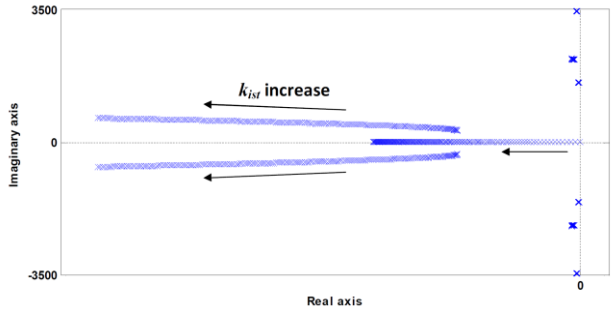

Fig. 5. Poles tracing of $G_v(s)/(1+G_v(s).G_{st}(s))$ for k_{ist} from 0 to

$$\omega_{rest} = \left(k_{pF} + \frac{k_{iF}}{s}\right)\cdot\left(\omega^*_{MG} - \omega_{MG}\right) \quad (9)$$

$$E_{rest} = \left(k_{pE} + \frac{k_{iE}}{s}\right)\cdot\left(E^*_{MG} - E_{MG}\right) \quad (10)$$

where k_{pF}, k_{iF}, k_{pE} and k_{iE} are parameters of PI controller, ω_{MG} and E_{MG} are the microgrid frequency and voltage amplitude, respectively, and ω^*_{MG} and E^*_{MG} are their reference values. ω_{rest} and E_{rest} are, respectively, the deviation of the frequency and voltage amplitude that should not exceed limits [1]- [2].

In order to analyze the system stability and to adjust the parameters of the secondary controller, a control model has been proposed in [12]. The diagram in Fig. 1 indicates the mentioned control model and transfer functions used in this control scheme. They are defined as follows:

$$G_{f\,\mathrm{sec}}(s) = k_{pF} + \frac{k_{iF}}{s} \quad (11)$$

$$G_{E\,\mathrm{sec}}(s) = k_{pE} + \frac{k_{iE}}{s} \quad (12)$$

$$G_d(s) = \frac{1}{s + 1.5\omega_s} \quad (13)$$

where $G_d(s)$ is the transfer function that models the delay of communication lines.

In secondary controller shown in Fig. 1, the ω_{sync} parameter also can be added to the frequency which satisfies frequency synchronization requirements when the system is connected to the grid [12].

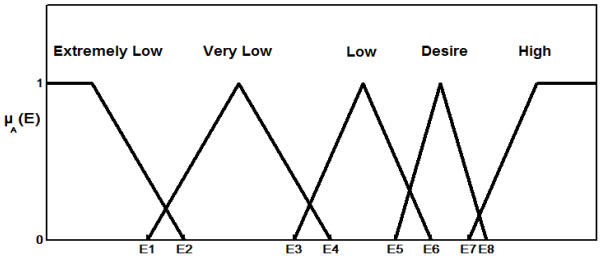

Fig.6. Membership function of triangular number $\mu_A(E)$ for different voltages magnitude.

4. Tertiary Control

In grid-connected mode, the power sharing between grid and microgrid, can be controlled by adjusting the frequency and voltage amplitude. By measuring the values of the active and reactive power flows in the point of common coupling (PCC), i.e., P_G and Q_G, and comparing them with their desired values P_G^* and Q_G^*, the PCC power flow can be controlled as below [29]:

$$\omega_{MGter}^* = \left(k_{pPg} + \frac{k_{iPg}}{s}\right)\cdot\left(P_G^* - P_G\right) \qquad (14)$$

$$E_{MGter}^* = \left(k_{pQg} + \frac{k_{iQg}}{s}\right)\cdot\left(Q_G^* - Q_G\right) \qquad (15)$$

The tertiary control block-diagram is shown in Fig. 1. It can be seen that the tertiary control is inactive when the microgrid is operating in islanded mode, and reference values of frequency and voltage (ω^*_{MG}, E^*_{MG}) in secondary controller are chosen by microgrid. In grid-connected mode, the tertiary controller generates these reference values (ω^*_{MGter}, E^*_{MGter}).

5. Control of Reactive Power Reference by Fuzzy Control Logic

In terms of large-signal disturbances such as short circuits and outage of lines, the new control loop by increasing the stability margin, has optimal performance in power sharing and maintaining the frequency and voltage. Nevertheless, when a heavy motor is started in microgrid, the voltage drops considerably and may exceeds the acceptable range. In this situation, the reactive power reference value should be floating. For generating the floating Q^*, use of the fuzzy logic is useful.

This stage of the control deals with adjusting the reference reactive power, Q^*. At the moment of motor starting, microgrid should bear heavy load and its outcome is a drastic voltage drop. Therefore, reactive power should be injected for compensation. The presented control scheme adjusts the set-point of the reactive power (Q^*) by using the fuzzy logic.

Fig. 6 shows the triangular membership functions with explanatory variables that considered for different voltage values of the microgrid, by using the equation of the membership function of a triangular number $\mu_A(X)$ defined in [35]-[37]. In provided fuzzy logic, E_i variables are the voltages amplitudes of the microgrid which are applied to fuzzy logic controller as non-fuzzy input. For different values of the voltage magnitude, each membership functions takes its own weight and generates the fuzzy input. Then in the next step, fuzzy inputs enter into a fuzzy inference system (FIS). The roles are defined in FIS so that when the voltage magnitude decreases, weight of the generated fuzzy output will be increased, and conversely. There is a direct relationship between the output fuzzy weight and the reactive power injection. Finally, after defuzzification, non-fuzzy output Δq is achieved. By applying a delay in Δq, the amount of the reactive power that must be added to the initial reference value of the reactive power (Q^*), is expressed by the following equation:

$$Q_{fu}^* = Q^* + \Delta Q, \qquad \Delta Q = \Delta q \cdot \left(\frac{1}{1+T_d s}\right) \qquad (16)$$

where, Q^*_{fu} is the new reference value of the reactive power which should be applied to the voltage droop equation. Δq is raw value of injective reactive power that after multiplying by the delay transfer function, its main value (ΔQ) will be obtained. By putting Q^*_{fu} in the voltage equation (1), we have:

$$E = E^* - G_Q(s)\cdot\left(Q - Q_{fu}^*\right) \qquad (17)$$

Fig. 7 shows the block diagram of the Q^* fuzzy control scheme.

6. Analysis and Simulation of Microgrid

In this section, a sample microgrid, including four DG units that are connected to the main grid in PCC, is modeled by SIMULINK/MATLAB software. Each DG unit has a local load. The single-line diagram of the microgrid can be seen in Fig. 8. The parameters of the microgrid and its hierarchical control are given in table 1.

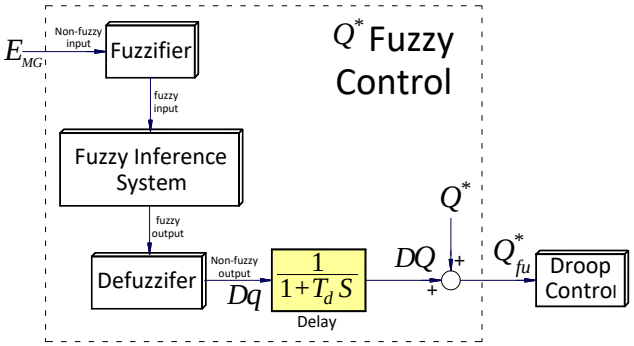

Fig. 7. Block diagram of Q^* fuzzy control scheme

TABLE. 1. Hierarchical Control Parameters

Items		Values	
Microgrid Parameters			
DG 1	14.7kVA	Load 1	11kW+j8.1kVAr
DG 2	23.5kVA	Load 2	17.2kW+j12.6kVAr
DG 3	13.6kVA	Load 3	9kW+j6.5kVAr
DG 4	28.4kVA	Load 4	20kW+j16.1 kVAr
System Voltage (L-L), f		415V, 50Hz	
V_{dc}		1000Vdc	
Z_{Line1}		0.3756+j0.1936Ω	
Z_{Line2}		0.1878+j0.0968Ω	
Z_{Line3}		0.1935+j0.1118Ω	
L, C		75.8mH, 50μF	
L_{o1}, L_{o2}, L_{o3}, L_{o4}		10.8, 6.94, 12.96, 5.9mH	
Primary/Inner Control Parameters			
k_{pP1}, k_{iP1}		0. 25e-3, 1.25e-6	
k_{pP2}, k_{iP2}		0. 161e-3, 0.8036e-6	
k_{pP3}, k_{iP3}		0. 3e-6, 1.5e-6	
k_{pP4}, k_{iP4}		0.136e-3, 0.682e-6	
k_{pQ1}, k_{pQ2}, k_{pQ3}, k_{pQ4}		0.725, 0.466, 0.87, 0.395	
R_{vi}, L_{vi}		1 Ω ,4e-4mH	
k_{pV}, k_{r1V}, k_{r5V}, k_{r7V},k_{r11V}		0.35, 400, 4, 20, 11	
k_{pI}, k_{r1I}, k_{r5I}, k_{r7I},k_{r11I}		0.7, 100, 30, 30, 30	
New Control Loop Parameters			
k_{pst}, k_{ist}		0.23, 0.11	
Secondary Control Parameters			
k_{pF}, k_{iF}, k_{pE}, k_{iE}		0.5e-3, 0.1, 0.1e-3, 0.11	
τ		50ms	
Tertiary Control Parameters			
k_{pPg}, k_{iPg}, k_{pQg}, k_{iQg}		0.7e-3, 9.8, 0.25e-3, 13	
Q^* Fuzzy Control Parameter			
T_d		23.5ms	

6.1. Operation in Islanded Mode

Fig. 9 shows the power sharing of the microgrid in islanded mode. In Fig. 10, the microgrid is influenced by a step load change. The load increase happens at the t=5s, so that the amount of 4kW adds to the load of the DG1 and 3kW adds to the load of the DG3, and it can be seen, this load increase is covered by DGs. In the next simulation, a symmetric three-phase short circuit fault, as a large disturbance, occurs in the middle of the line between DG1 and DG2. The fault happens at t=4s and it clears after six cycles. It has been shown, when microgrid is controlled without using the new control loop, after fault clearance the voltage is highly oscillatory and cannot return to its nominal value (Fig. 11). In this situation, voltage and current control loops

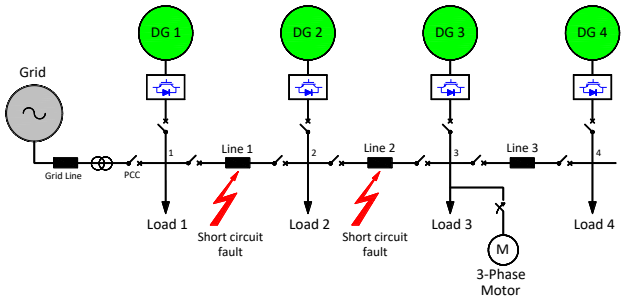

Fig. 8. Single line diagram of studied microgrid.

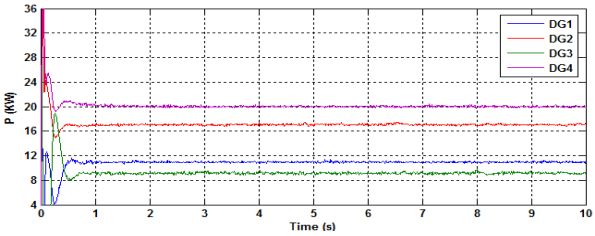

Fig. 9. Power sharing of microgrid in islanded mode.

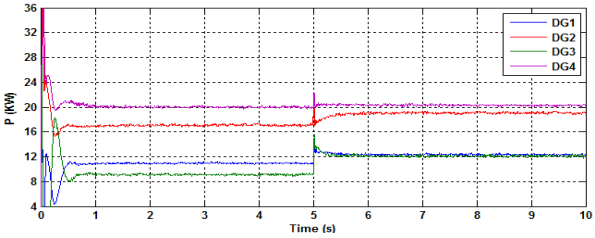

Fig. 10. Power sharing of microgrid in islanded mode - step load change.

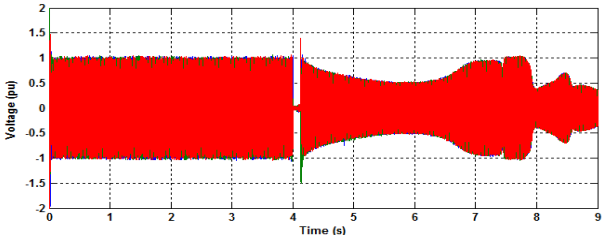

Fig. 11. Voltage waveform of microgrid (without using new control loop) in islanded mode and symmetric 3-phase fault condition.

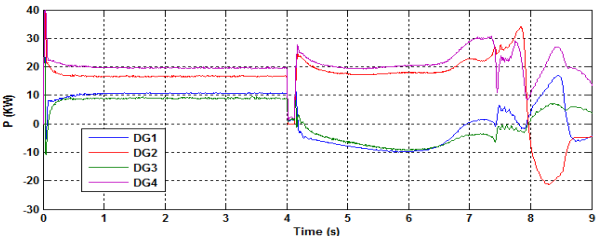

Fig. 12. Power sharing of microgrid (without using new control loop) in islanded mode and symmetric 3-phase fault condition.

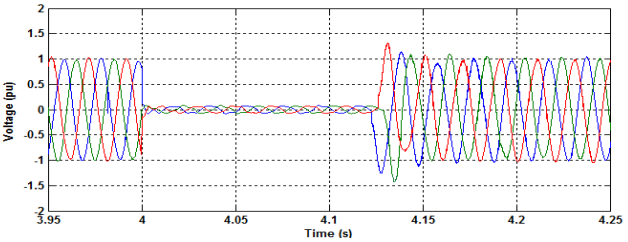

Fig. 13. Voltage waveform of microgrid (with proposed control scheme) in islanded mode and symmetric 3-phase fault condition.

cannot be converged and due to the ΔE is high, secondary voltage control cannot compensate voltage deviation. Also it can be seen in Fig. 12, the power sharing loses its stability. Whereas, by adding the new control loop the microgrid voltage restore to nominal value, after fault clearance (Fig. 13). Likewise, the frequency waveform in this situation is shown in Fig. 14. As can be seen in Fig. 15, the microgrid power sharing continues without any problem, by using the provided control scheme. The output current

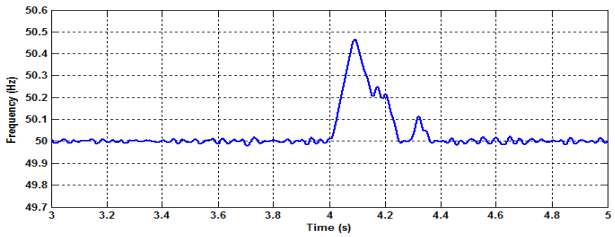

Fig. 14. Frequency of microgrid (with proposed control scheme) in islanded mode and symmetric 3-phase fault condition.

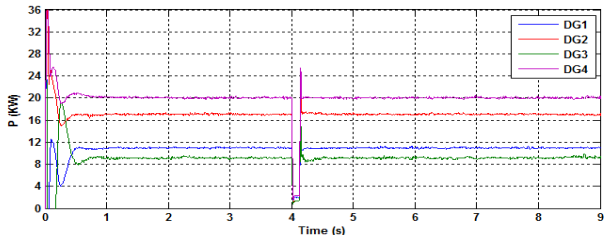

Fig. 15. Power sharing of microgrid (with proposed control scheme) in islanded mode and symmetric 3-phase fault condition.

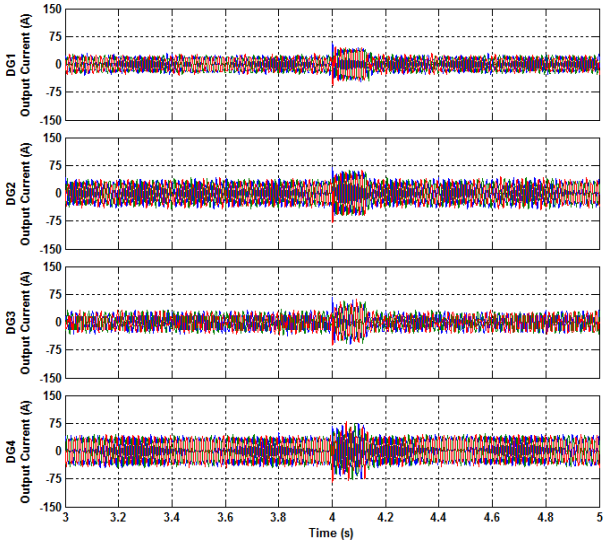

Fig. 16. Output current waveforms of the DGs (with proposed control scheme) in islanded mode and symmetric 3-phase fault condition.

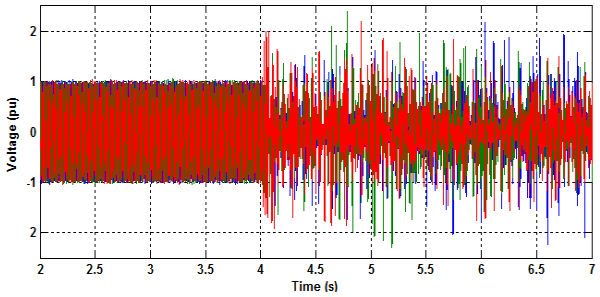

Fig. 17. Voltage waveform of microgrid (without using new control loop) in islanded mode and 1-phase to ground fault condition.

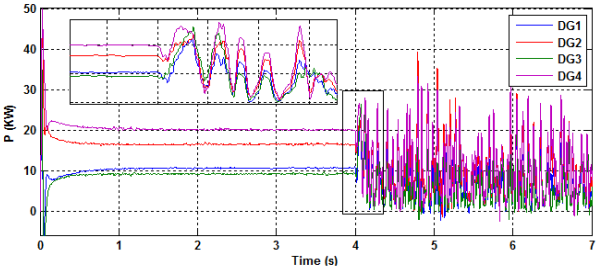

Fig. 18. Power sharing of microgrid (without using new control loop) in islanded mode and 1-phase to ground fault condition.

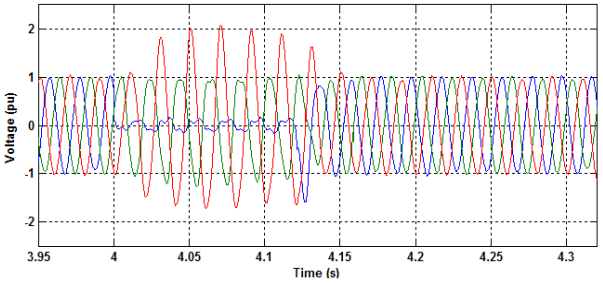

Fig. 19. Voltage waveform of microgrid (with proposed control scheme) in islanded mode and 1-phase to ground fault conditions.

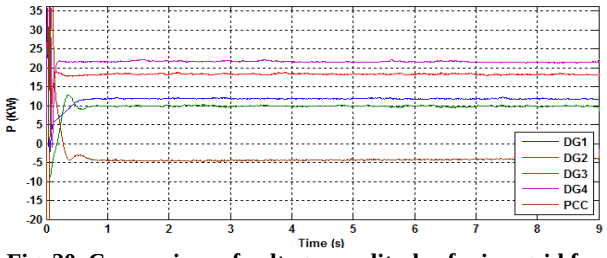

Fig. 20. Comparison of voltage amplitude of microgrid for three mentioned cases in motor starting mode.

waveforms of the DGs in the fault conditions are shown in Fig. 16.

The single-phase to ground short circuit not only is a severe disturbance but also makes serious unbalance in the system. Thus, this is important that the microgrid has an acceptable performance in dealing with this event. In the next step, a single-phase to ground fault is

TABLE. 2. Comparison of Microgrid Performance for Different Control Schemes

Control Scheme	Disturbance Description	
	Small-signal events: Step load	Large-signal disturbance: Short circuit fault
Hierarchical Control:	Good performance	Unstable, Bad performance
Hierarchical Control+ New Control Loop:	Good performance	Good performance
Hierarchical Control+ New Control Loop+ Q^* Fuzzy Controller:	Good performance	Good performance

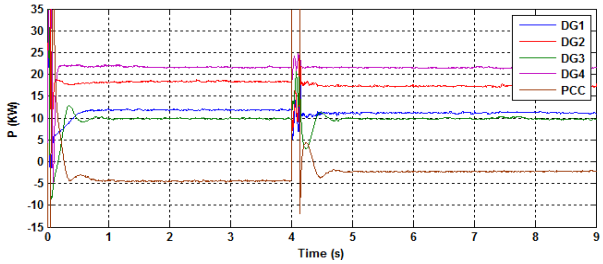

Fig. 21. Microgrid (with the proposed control scheme) power sharing in grid-connected mode-1-phase to ground fault conditions.

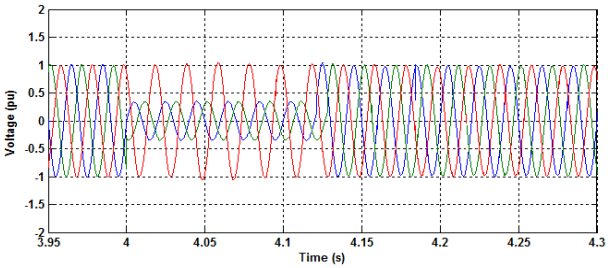

Fig. 22. Voltage waveform of the microgrid (with the proposed control scheme) in grid-connected mode- 1-phase to ground fault conditions.

simulated in the middle of the line between DG1 and DG2 at t=4s, and after six cycles breaker isolates the line from the circuit. The results are shown in Figs. 17 to 20. It can be seen the good performance of the proposed control scheme. The microgird hierarchical control without using new control loop cannot cover the large-signal disturbance and it will be unstable.

6.2. Operation in Grid-connected Mode

In grid-connected mode, the hierarchical control scheme is completed with the presence of the tertiary control. Fig. 20 indicates power sharing among microgrid, load and main grid. The microgrid supplies the power of local loads and also injects 4.5kW power to the main grid. In Fig. 21 and Fig. 22, a single-phase to ground fault is simulated in this mode. The single-phase to ground fault occurs in the line between DG2 and DG3 at t=4s and then after six cycles breaker disconnect the line2 from the circuit. In this situation, DG3 and DG4 are isolated from the network and supply their local load. After fault clearance, the voltages are stable and power sharing continues between loads, microgrid and grid, as before the fault (Fig. 21). In Fig. 22, the voltage waveform of the microgrid is shown during the fault period.

The general results of microgrid control performance for different control schemes have been listed in table 2. It can be seen, the control scheme with using new control loop and Q^* fuzzy controller, have good performance in all simulated conditions.

7. Conclusion

The microgrid hierarchical control scheme is improved by two innovative strategies, adding the new control loop and generating the float reactive power reference value. The new control loop based on PI controller have a great effect on increasing stability margin by moving the poles. Also a compromise is made between reducing effectiveness of resonant terms in tracking harmonics, and increasing stability. Floating Q^* strategy runs by fuzzy logic controller in the voltage droop equation. So that, the Q^* fuzzy logic controller compensates drastic changes in the microgrid voltage amplitude. The presented control scheme maintains stability of the frequency and voltage of the microgrid against large-signal disturbance such as 1-phase and 3-phase to guard fault. Simulations results show that by using the mentioned control strategies, micrigrid have desired performance in facing large-signal disturbances and the load sharing remains unchanged after fault clearance.

References

[1] J.M. Guerrero, M. Chandorkar, T. Lee and P.C. Loh, "Advanced Control Architectures for Intelligent Microgrids—Part I: Decentralized and Hierarchical Control", IEEE Trans. on Industrial Electronics, Vol. 60, No. 4 , pp. 1254–1262, April 2013.

[2] C. Dou; M. Lv; T. Zhao; Y. Ji; H. Li, "A Decentralised coordinated control of microgrid based on multi-agent system", IET Generation, Transmission & Distribution, Volume 9, Issue 16, 03 December 2015, p. 2474 – 2484.

[3] Q. Fu, A. Nasiri, A. Solanki, A. Bani-Ahmed, L. Weber and V. Bhavaraju, "Microgrids: Architectures, Controls, Protection, and Demonstration", Electric Power Components and Systems, Volume 43, Issue 12, July 2015, pages 1453-1465.

[4] P. Hasanpor Divshali, A. Alimardani, S.H. Hosseinian, M. Abedi, "Decentralized Cooperative Control Strategy of Microsources for Stabilizing Autonomous VSC-Based Microgrids", IEEE Trans. on Power Systems, Vol. 27, No. 4 pp. 1949–1959, Nov. 2012.

[5] F.A. Bhuiyan, A.n. Yazdani, S.L. Primak, P.C. Loh, "Optimal sizing approach for islanded microgrids", IET Renewable Power Generation, Volume 9, Issue 2, 2015 , p. 166 – 175.
[6] J. A. P. Lopes, C. L. Moreira, and A. G. Madureira, "Defining control strategies for microgrids islanded operation,", IEEE Trans. on Power Systems, Vol. 21, No. 2, pp. 916–924, May 2006.
[7] M.M. Rezaei and J. Soltani, "A Robust control of an islanded multi-bus microgrid based on input–output feedback linearisation and sliding mode control", IET Generation, Transmission & Distribution, Volume 9, Issue 15, 19 November 2015, p. 2447 – 2454.
[8] R. Maheshwari, Gh. Gohil, L. Bede, S. Munk-Nielsen, "Analysis and modelling of circulating current in two parallel-connected inverters" , IET Power Electronics, Volume 8, Issue 7, 2015 , p. 1273 – 1283.
[9] M.C. Chandorkar, D.M. Divan, and R. Adapa, "Control of parallel connected inverters in standalone ac supply systems," IEEE Trans. on Industry Applications, Vol. 29, No. 1, pp. 136–143, Jan./Feb. 1993.
[10] A. Bidram, A. Davoudi, "Hierarchical Structure of Microgrids Control System", IEEE Trans. on Smart Grid, Vol. 3, No. 4, pp. 1963–1976, Dec. 2012
[11] Pogaku N., Prodanovic M., Green T.C., "Modeling, Analysis and Testing of Autonomous Operation of an Inverter-Based Microgrid", IEEE Trans. on Power Electronics, Vol. 22, No. 2, pp. 613–625, March 2007.
[12] J.C. Vasquez, M. Guerrero, M.Savaghebi, J. Eloy-Garcia R. Teodorescu "Modeling, Analysis, and Design of Stationary-Reference-Frame Droop-Controlled Parallel Three-Phase Voltage Source Inverters", IEEE Trans. on Industrial Electronics, Vol. 60, No. 4, pp. 1271–1280 April 2013.
[13] R. Majumder, B. Chaudhuri, A. Ghosh, R. Majumder, G. Ledwich, F. Zare, "Improvement of stability and load sharing in an autonomous microgrid using supplementary droop control loop", IEEE Trans. on Power Systems, Vol. 25, No. 2, pp. 796–808, May 2010.
[14] C. N. Rowe, T. J. Summers, R. E. Betz, D. J. Cornforth, T. G. Moore, "Arctan Power–Frequency Droop for Improved Microgrid Stability", IEEE Trans. on Power Electronics, Vol. 28, No. 8, pp. 3747–3759, Aug. 2013.
[15] R. Majumder A. Ghosh G. Ledwich F. Zare, "Load sharing and power quality enhanced operation of a distributed microgrid", IET Renewable Power Generation, Vol. 3, No. 2, pp. 109–119, June 2009.
[16] F. Luo, Y. M. Lai, K. H. Loo, Chi K. Tse, Xinbo Ruan, "A Generalized Droop-Control Scheme for Decentralized Control of Inverter-Interfaced Microgrids" Circuits and Systems (ISCAS), 2013 IEEE International Symposium on, pp. 1320-1323, 10.1109/ISCAS.2013.6572097.
[17] J. Rocabert, A. Luna, F. Blaabjerg, P. Rodriguez "Control of Power Converters in AC Microgrids", IEEE Trans. on Power Electronics, Vol. 27, No. 11, pp. 4734–4749, Nov. 2012.
[18] Kamwa I., Grondin R., Hebert Y., "Wide-Area Measurement Based Stabilizing Control of Large Power Systems-A Decentralized/Hierarchical Approach", IEEE Trans. on Power Systems, Vol. 16, No. 1, pp. 136–153, Feb. 2001.
[19] R. Majumder, G. Ledwich, A. Ghosh, "Droop Control of Converter-Interfaced Microsources in Rural Distributed Generation", IEEE Trans. on Power Delivery, Vol. 25, No. 4, pp. 2768–2778, Oct. 2010.
[20] Juan Carlos V´asquez Quintero, "Decentralized Control Techniques Applied to Electric Power Distributed Generation in Microgrids", PhD Thesis, Universitat Politècnica de Catalunya, 2009.
[21] A. H. Etemadi, E. J. Davison, R. Iravani, "A Decentralized Robust Control Strategy for Multi-DER Microgrids—Part I: Fundamental Concepts" IEEE Trans. on Power Delivery, Vol. 27, No. 4, pp. 1843–1853, Oct. 2012.
[22] A. H. Etemadi, E. J. Davison, R. Iravani, "A Decentralized Robust Control Strategy for Multi-DER Microgrids— Part II: Performance Evaluation", IEEE Trans. on Power Delivery, Vol. 27, No. 4, pp. 1854–1861, Oct. 2012.
[23] M. Babazadeh, H. Karimi, "Robust Decentralized Control for Islanded Operation of a Microgrid" Power and Energy Society General Meeting, 2011 IEEE, pp. 1-8, 10.1109/PES.2011.6039646.
[24] Y. Abdel-Rady, I. Mohamed, E. F. El-Saadany "Adaptive Decentralized Droop Controller to Preserve Power Sharing Stability of Paralleled Inverters in Distributed Generation Microgrids", IEEE Trans. on Power Electronics, Vol. 23, No. 6, pp. 2806–2816, Nov. 2008.
[25] R. Majumder, A. Ghosh, G. Ledwich, F. Zare "Angle droop versus frequency droop in a voltage source converter based autonomous microgrid," in Proc. IEEE PES Gen. Meeting, 2009, pp. 1–8.
[26] M. Savaghebi, A. Jalilian, J. C. Vasquez, J. M. Guerrero "Secondary Control Scheme for Voltage Unbalance Compensation in an Islanded Droop-Controlled Microgrid", IEEE Trans. on Smart Grid, Vol. 3, No. 2, pp. 797–807, June 2012.
[27] M. Savaghebi, A. Jalilian, J. C. Vasquez, J. M. Guerrero "Secondary Control for Voltage Quality Enhancement in Microgrid", IEEE Trans. on Smart Grid, Vol. 3, No. 4, pp. 1893–1902, Dec. 2012.
[28] F. Katiraeiet, M. R. Iravani, "Power management strategies for a microgrid with multiple distributed generation units", IEEE Trans. on Power Systems, Vol. 21, No. 4, pp. 1821–1831, Nov 2006.
[29] F. Katiraeiet, M. R. Iravani, N. Hatziargyriou, A. Dimeas, "Microgrids management", IEEE Power and Energy Magazine, vol. 6, No. 3, pp. 54–65, May–June 2008.
[30] J. M. Guerrero, J. C. Vásque, R. Teodorescu "Hierarchical control of droop-controlled ac and dc microgrids—A general approach toward standardization", IEEE Trans. on Industrial Electronics, Vol. 58, No. 1, pp. 158–172, Jan. 2011.
[31] H. Han, Y. Liu, Y. Sun, M. Su, M. Guerrero, "An Improved Droop Control Strategy for Reactive Power Sharing in Islanded Microgrid", IEEE Transactions On Power Electronics, Vol. 30, NO. 6, JUNE 2015.
[32] W. De Souza, M. Mendes, L. Lopes "Power sharing control strategies for a three-phase microgrid in different operating condition with droop control and damping factor investigation", IET Renew. Power Gener. 2015, Vol. 9, Iss. 7, pp. 831–839.
[33] H. Han, X. Hou, J. Yang, J. Wu, M. Su, M. Su, M. Guerrero, "Review of Power Sharing Control Strategies for Islanding Operation of AC Microgrids", Ieee Transactions On Smart Grid, Vol. 7, NO. 1, Jan. 2016.
[34] W. C. Duesterhoeft, Max W. Schulz and Edith Clarke "Determination of Instantaneous Currents and Voltages by Means of Alpha, Beta, and Zero Components".

Trans. of the American Institute of Electrical Engineers, Vol. 70, No. 2, pp. 1248–1255, july 1951.
[35] G. Chen, T. T. Pham, J. J. Weiss, " Fuzzy Modeling of Control Systems" , IEEE Trans. on Aerospace and Electrical Systems, Vol. 31, No. 1, pp. 414–429, Jan. 1995.
[36] G. Feng, "A Survey on Analysis and Design of Model-Based Fuzzy Control Systems", IEEE Trans. on Fuzzy Systems, Vol. 14, No. 5, pp. 676–697, Oct 2006.
[37] V. Belton, TJ. Stewart. ”Multiple criteria decision analysis: an integrated approach. ” USA: Kluwer Academic Publisher; 2002.